

Thermal defect annealing of swift heavy ion irradiated ThO₂



Raul I. Palomares^a, Cameron L. Tracy^b, Joerg Neufeind^c, Rodney C. Ewing^b, Christina Trautmann^{d,e}, Maik Lang^{a,*}

^a Department of Nuclear Engineering, University of Tennessee, Knoxville, TN 37996, USA

^b Department of Geological Sciences, Stanford University, Stanford, CA 94305, USA

^c Chemical and Engineering Materials Division, Spallation Neutron Source, Oak Ridge National Laboratory, Oak Ridge, TN 37831, USA

^d GSI Helmholtzzentrum für Schwerionenforschung, 64291 Darmstadt, Germany

^e Technische Universität Darmstadt, 64287 Darmstadt, Germany

ARTICLE INFO

Article history:

Received 26 March 2017

Received in revised form 2 May 2017

Accepted 3 May 2017

Available online 19 May 2017

Keywords:

ThO₂

Swift heavy ions

Defects

Neutron total scattering

Raman spectroscopy

Annealing

ABSTRACT

Isochronal annealing, neutron total scattering, and Raman spectroscopy were used to characterize the structural recovery of polycrystalline ThO₂ irradiated with 2-GeV Au ions to a fluence of 1×10^{13} ions/cm². Neutron diffraction patterns show that the Bragg signal-to-noise ratio increases and the unit cell parameter decreases as a function of isochronal annealing temperature, with the latter reaching its pre-irradiation value by 750 °C. Diffuse neutron scattering and Raman spectroscopy measurements indicate that an isochronal annealing event occurs between 275–425 °C. This feature is attributed to the annihilation of oxygen point defects and small oxygen defect clusters.

© 2017 Elsevier B.V. All rights reserved.

1. Introduction

ThO₂ is isostructural with UO₂ and can be used as a nuclear fuel in which the ²³²Th breeds fissile ²³³U [1]. Thorium-based fuels offer several advantages over conventional uranium-based fuels. Examples include a high chemical durability, improved thermophysical properties, and competitive neutronic properties [2]. Despite these advantages and international interest in thorium-based fuels, there exist only few data on the structural stability of ThO₂ under the high-temperature irradiation conditions encountered in nuclear reactors. In order to better understand the evolution of important physiochemical properties and the performance of potential advanced nuclear fuels under these operational conditions, it is important to understand the stability and kinetics of irradiation-induced defects in ThO₂.

Swift heavy ion irradiation is a valuable tool for investigating the behavior of materials in response to highly ionizing radiation, such as from fission-fragment irradiation, which occurs continuously in nuclear fuels during use. Unlike low energy ions and neutrons, swift heavy ions with specific energy >1 MeV/nucleon generate dense electronic excitations in target

materials via inelastic electronic energy loss [3]. Electronic excitations can yield a variety of permanent material modifications. In ThO₂, dense electronic excitation typically results in the formation of isolated point defects and small defect clusters [4] as is typical of other fluorite-structure oxides, such as CeO₂ [5–7]. Studies have also shown that ThO₂ exposed to energetic ion irradiation can undergo dramatic color changes from white to blue [8,9]. The presence of these unique modifications, attributed to radiative electron-hole recombination [9] and the subsequent formation of color centers [8,10], suggests that electronic structure modifications, such as self-trapped exciton formation and decay, may play an important role in the damage accumulation process under swift heavy ion irradiation.

In ThO₂, the charge state of thorium is predominantly fixed in the Th⁴⁺ state. The absence of multiple oxidation states for Th, which is not the case for cations in UO₂ and CeO₂, is thought to improve its radiation tolerance by eliminating redox-enhanced disorder [11]. However, it remains unclear how ThO₂ accommodates irradiation-induced defects without exhibiting geometric frustration as a result of charge balance constraints of the fixed tetravalent state. This study investigates the annealing mechanisms that occur during isochronal annealing of ThO₂ irradiated by swift heavy ions. Neutron total scattering and Raman spectroscopy measurements provide insights into the structural

* Corresponding author.

E-mail address: mlang2@utk.edu (M. Lang).

features that distinguish the defect structure of ThO_2 from isostructural CeO_2 and UO_2 .

2. Experimental methods

Neutron total scattering measurements often require a large sample volume as compared with X-ray scattering measurements because of the lower fluxes typically associated with neutron sources. This is challenging for investigating ion irradiation effects because the penetration depth of MeV ions is typically only a few tens of microns. In order to obtain sufficient homogeneously-irradiated sample for neutron total scattering measurements, pressed powder was irradiated by using specially designed aluminum powder sample holders with circular indentations that are 75 μm thick and 1 cm in diameter. Additional details regarding these holders and the ion irradiation sample preparation are provided elsewhere [12]. Microcrystalline ThO_2 powder was irradiated at the X0 beamline of the Universal Linear Accelerator (UNILAC) at the GSI Helmholtz Center for Heavy Ion Research in Darmstadt, Germany. The irradiations were performed at room temperature and under vacuum with 2-GeV Au ions to a fluence of 1×10^{13} ions/ cm^2 . The ion energy loss in this energy regime is primarily electronic with negligible nuclear energy loss. Energy loss calculations were performed using the SRIM-2008 code [13] assuming 60% theoretical density of solid ThO_2 ($\rho_0 = 10 \text{ g/cm}^3$), following the method of Lang et al. [14]. The SRIM results indicate that for the given experimental parameters, the mean ion range in the low-density powder ThO_2 samples is about 89 μm . This value exceeds the thickness of the pressed powder samples ($\sim 75 \mu\text{m}$) meaning that the ions penetrated the entire sample volume without being implanted. The linear electronic energy loss calculated using SRIM and averaged over the entire sample thickness is $42 \pm 7 \text{ keV/nm}$. The uncertainty in this value represents the upper and lower bounds to the electronic energy loss in the sample. The calculated nuclear energy loss is negligible within the material.

After irradiation, the compacted powder was removed from the sample holders using a blunt tipped needle. Approximately 100 mg of irradiated powder was recovered. The powder was loaded into a thin-walled (0.38 mm) quartz NMR tube, which was placed inside a vanadium can coupled to an ILL-type vacuum furnace. The air was not evacuated from the sealed sample can prior to loading it into the furnace; therefore, the annealing was essentially performed in an air atmosphere. The irradiated sample and an unirradiated reference sample were annealed and measured at the Nanoscale-Ordered MAterials Diffractometer (NOMAD) beamline at the Spallation Neutron Source (SNS) at Oak Ridge National Laboratory [15]. The temperature profile used for the isochronal annealing experiment is illustrated in Fig. 1. In short, each annealing temperature was maintained for 20 min and the ramps/quenches to/from the target annealing temperatures were performed as rapidly as possible ($\sim 10 \text{ }^\circ\text{C/min}$ ramp). After quenching from each temperature step, neutron scattering data were collected for 1 h at $80 \text{ }^\circ\text{C}$. Sluggish cooling rates associated with the vacuum furnace precluded the collection of data at temperatures much lower than $80 \text{ }^\circ\text{C}$.

The NOMAD detectors were calibrated with diamond powder, and a silicon standard was utilized to derive the instrument parameters for Rietveld refinement. Rietveld refinement of diffractograms was performed with GSAS-II [16] using only data from the highest resolution detector bank. The diffractograms were fit with the fluorite structure model (space group $Fm-3m$). In order to derive the pair distribution functions (PDFs), data from all detector banks were combined. The structure factors, $S(Q)$, were obtained by normalizing the sample scattering intensity to the scattering from a solid vanadium rod and subtracting background scattering

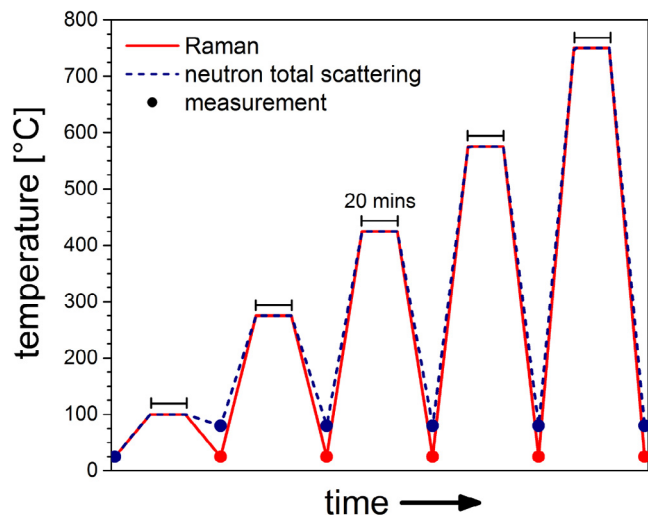


Fig. 1. Temperature profiles used for the neutron total scattering and Raman isochronal annealing experiments. The slopes of the lines in the heating and cooling stages are for illustrative purposes only and are not representative of the actual temperature ramp and quench rates. One-hour measurements, denoted by filled circles, were only performed after quenching from high temperatures.

obtained by measuring an empty NMR tube inside a vanadium can at $80 \text{ }^\circ\text{C}$. The PDFs, $G(r)$, were calculated by Fourier transform of the $S(Q)$ functions with $Q_{min} = 0.1 \text{ \AA}^{-1}$ and $Q_{max} = 25 \text{ \AA}^{-1}$:

$$G(r) = r \left(A \int_{Q_{min}}^{Q_{max}} Q[S(Q) - 1] \sin(Qr) dQ \right)$$

where Q is the scattering vector defined as $Q = 4\pi/\lambda \sin\theta$, r is the real-space distance in angstroms, and A is an arbitrary scaling factor.

The PDFs were analyzed by means of small-box refinement performed with PDFgui [17]. Small-box refinement is a Rietveld-type method in which the properties (e.g., position, atomic displacement parameters, etc.) of atoms in a box the size of one or more unit cells are adjusted to reproduce the experimental PDF [17]. A small amount of parasitic scattering from SiO_2 was unavoidable because the sample volume was so small compared to the quartz NMR tube. This resulted in SiO_2 peaks appearing at low r ($r < 3 \text{ \AA}$) in the PDFs of the irradiated sample. The peaks are attributed to the first nearest-neighbor (1-NN) $\langle\text{Si-O}\rangle$ correlation at $\sim 1.6 \text{ \AA}$ and the 1-NN $\langle\text{O-O}\rangle$ correlation at $\sim 2.6 \text{ \AA}$. In order to take these peaks into account, the PDFs were analyzed with a two-phase refinement consisting of crystalline ThO_2 ($Fm-3m$) and amorphous SiO_2 . The amorphous SiO_2 was modeled using the PDF of crystalline quartz SiO_2 that was truncated at low r (3–10 \AA). The best results were obtained when the SiO_2 PDF was truncated at 3 \AA . This indicates that the SiO_2 contribution to the higher r regions is negligible and the unit cell parameters derived from full-profile (1–50 \AA) small-box refinement are accurate.

Micro-Raman measurements were performed using a Horiba LabRAM HR Evolution instrument equipped with a 532 nm excitation laser source and a liquid nitrogen-cooled charge coupled device detector. The laser power was maintained at 0.05 mW throughout the experiment in order to avoid heating and laser-induced defect annealing of the irradiated sample. Several particles of the irradiated ThO_2 powder were sampled prior to annealing in order to verify that the measured spectra were representative of the entire sample. The isochronal anneal was performed *ex situ* in an alumina furnace in air, with the temperature profile shown in Fig. 1. After quenching from each annealing temperature, the samples were left to cool for at least 15 min prior to collecting the Raman spectra. All spectra were collected from an identical

spot on the sample using the same measurement conditions. This ensured that the spectra collected were directly comparable. Peak fitting of the Raman spectra was performed with Pseudo-Voigt peak profiles using DatLab [18]. Prior to peak fitting, the background was subtracted and the spectra were normalized to the intensity of the main F_{2g} peak. The reported peak position values represent the average of 10 peak fits and the reported uncertainty represents the standard deviation of the mean.

3. Results

3.1. Unit cell parameter

Neutron total scattering measurements provide information about the structure over multiple length scales. This includes information from both crystalline domains with long-range ordering (Bragg scattering) and non-periodic features, such as defects (diffuse scattering). Prior to analyzing the diffuse scattering, the evolution of the unit cell parameter was analyzed in order to characterize the average structure of the irradiated sample. Rietveld refinement of the neutron diffraction patterns confirmed that ThO_2 maintains the fluorite structure after irradiation (Fig. 2). This is consistent with X-ray diffraction (XRD) studies showing that ThO_2 does not undergo amorphization or phase transformations under swift heavy ion irradiation [11,19–21].

The accumulation of ion-induced defects in radiation tolerant fluorite-structured materials typically results in a decrease in Bragg peak intensities and an increase in the unit cell parameter (i.e., swelling) [11]. These effects are attributed to the displacement of some atoms to interstitial positions, which results in the formation of defects and the expansion of the structure to accommodate the extra volume occupied by these defects. Thermal annealing of an irradiated sample typically induces structural recovery, reversing these effects. As the irradiated material is annealed, the unit cell parameter recovers as a function of isochronal annealing temperature. This decrease in unit cell parameter is driven by the annihilation of irradiation-induced defects. Fig. 3 shows the relative change in the unit cell parameter for irradiated ThO_2 as a function of isochronal annealing temperature, as determined from neutron diffraction, neutron PDF analysis, and XRD (see Fig. 3 caption).

The unit cell parameter of the irradiated sample prior to annealing ($a = 5.6003 \text{ \AA}$) shows a volume increase of $\sim 0.055\%$ relative to

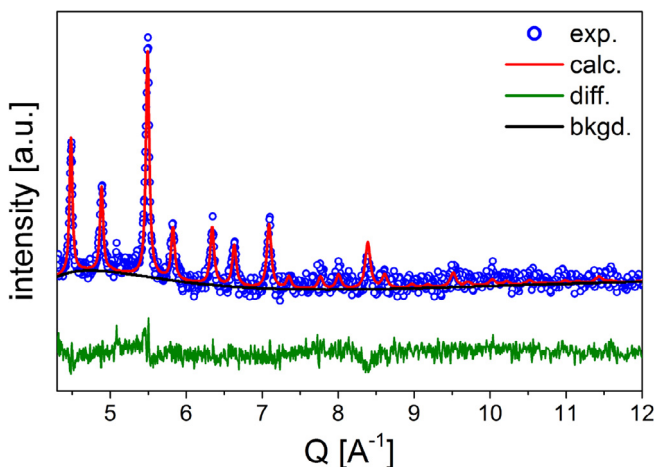


Fig. 2. Rietveld refinement of the neutron diffraction pattern for the irradiated ThO_2 sample prior to annealing. The diffraction pattern of the irradiated sample (blue circles) was fit using a fluorite-structure model (red line). The background (black line) is high because of the small sample volume. The difference curve (green line) illustrates the difference between the data and the fit. (For interpretation of the references to colour in this figure legend, the reader is referred to the web version of this article.)

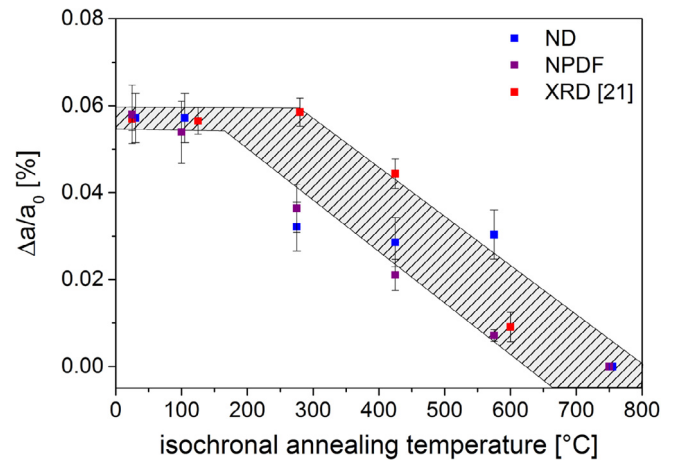


Fig. 3. Relative change in unit cell parameter derived from Rietveld refinement of the neutron diffraction (ND) patterns and small-box refinement of the neutron pair distribution functions (NPDF). The data are compared to the X-ray diffraction (XRD) results from Ref. [21]. The XRD values exhibit a similar trend (i.e., plateau below $\sim 300 \text{ }^\circ\text{C}$ and decreasing trend above $\sim 300 \text{ }^\circ\text{C}$), but with different relative magnitude. Therefore, the XRD data points were all multiplied by a constant (2.8) along the vertical axis in order to highlight the similarity in trend between the two data sets. The shaded region is used to guide the eye.

the unirradiated sample ($a = 5.5971 \text{ \AA}$). This is in close agreement with the value of $\sim 0.045\%$ reported by Tracy et al. for ThO_2 irradiated with 945-MeV Au ions to the same fluence [11]. The unit cell shows little change between 25–100 $^\circ\text{C}$, but begins to decrease monotonically after annealing at 275 $^\circ\text{C}$. After heating the irradiated sample to 750 $^\circ\text{C}$, the unit cell recovers to the pre-irradiation value. The overall recovery trend is similar to that reported for ThO_2 irradiated with 945-MeV Au ions and characterized by XRD [21], also shown in Fig. 3, especially near the initial and end points. Assuming that 2-GeV Au and 945-MeV Au irradiations yield similar types of defects in ThO_2 , both data sets should exhibit similar isochronal defect annealing behavior. There is larger scatter in the data from the 2-GeV Au irradiations for the temperature steps between 275 and 575 $^\circ\text{C}$; however, this may be attributed to the lower number of data points and the lower neutron diffraction signal-to-noise ratio that resulted from the small irradiated sample volume, relative to the volumes typically required for neutron scattering experiments. The trend derived from small-box refinement of the PDFs shows better agreement with the XRD data.

Fig. 4 shows the small-box refinement results for unirradiated and irradiated ThO_2 , as well as irradiated ThO_2 after annealing for 20 min at 750 $^\circ\text{C}$. After irradiation, the peaks in the PDF broaden and shift. The peak broadening is attributed to the accumulation of heterogeneous microstrain, atomic disordering, and the accumulation of point defects. The peak shifts are caused by changes in the unit cell parameter. The PDFs were all fit well with the fluorite structure, as indicated by the small intensities of the difference curves. This shows that the structural changes occurring after irradiation and during annealing are subtle. The PDF analysis did not show any systematic changes in atomic displacement parameters. However, the derived unit cell parameters yield a trend similar to the trend determined from neutron diffraction Rietveld refinement (Fig. 3). The unit cell parameters from diffraction and PDF analyses typically differ because of the finite measurement range and the resolution of the instrument [22].

3.2. Diffuse scattering

Further analysis of the Bragg scattering data can be performed by taking the derivative of the $\Delta a/a_0$ vs. temperature curve shown in Fig. 3. This “derivative function” will typically exhibit peaks,

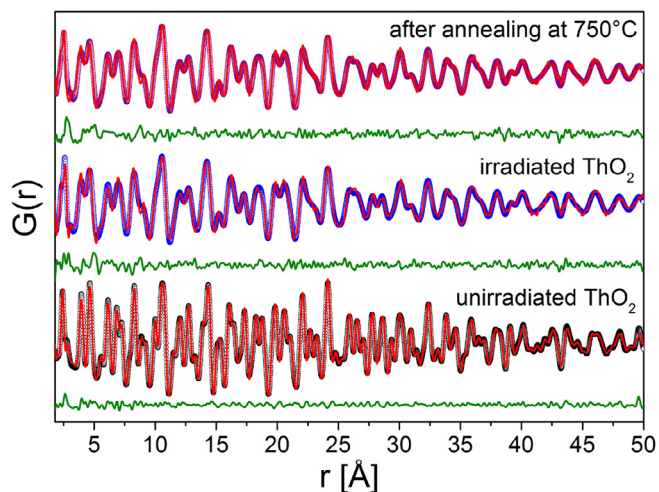


Fig. 4. Small-box refinements of the pair distribution functions (PDFs) of unirradiated ThO₂, irradiated ThO₂ before annealing, and irradiated ThO₂ after annealing at 750 °C for 20 min. The PDFs (colored circles) were fit with a fluorite-structure model (red lines). The difference curves (green lines) illustrate the difference between the data and the fit. (For interpretation of the references to colour in this figure legend, the reader is referred to the web version of this article.)

which correspond to distinct annealing stages [23]. These annealing stages represent intrinsic defect recovery processes with unique activation energies [24]. However, such analysis requires the collection of numerous data points in order to be reliable, which was unfeasible considering the slow cooling rate of the ILL-type vacuum furnace installed at the neutron beamline. In order to circumvent this issue, the identification of distinct recovery processes was instead performed by monitoring the intensity of the diffuse scattering, which is representative of atomic disorder [25].

Fig. 5 shows the total scattering function, $S(Q)-1$, for the irradiated sample in the range $1 < Q < 4 \text{ \AA}^{-1}$ for various annealing temperatures. The Q -range was cropped to highlight the region with the largest change in diffuse scattering. Anomalous diffuse scattering in the range $1 < Q < 4 \text{ \AA}^{-1}$ has previously been observed in isostructural CeO₂ [26] and compounds with the fluorite-derivative pyrochlore structure [27,28]. After irradiation and prior to annealing, the level of diffuse scattering is high. The diffuse scat-

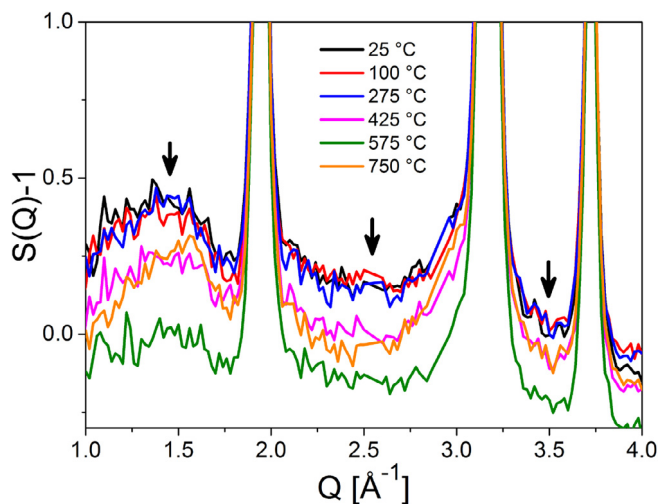


Fig. 5. Total scattering function, $S(Q)-1$, for irradiated ThO₂ as a function of isochronal annealing temperature in the region $1 < Q < 4 \text{ \AA}^{-1}$. The black arrows point to the diffuse scattering referred to in the text.

tering suggests that the sample has considerable atomic disorder and/or a large concentration of defects. Upon heating, the diffuse scattering decreases. Between 25–275 °C there is negligible change in the diffuse scattering, but between 275–425 °C the diffuse scattering abruptly decreases indicating that ThO₂ has a distinct annealing stage between 275–425 °C. Further annealing to 575 °C decreases the diffuse scattering even more. However, it is unclear if the second decrease is indicative of a second annealing stage, or if the diffuse scattering decreases linearly after 425 °C. Heating up to 750 °C subsequently raises the diffuse scattering to the level observed after the 425 °C temperature step.

Similar to the unit cell behavior, the temperature-dependence of the diffuse scattering is qualitatively in agreement with prior observations. Prior work has shown that ThO₂ irradiated with 945-MeV Au ions exhibits at least one annealing stage (*i.e.*, a peak in the derivative function) beginning around 200–300 °C [21]. The large width (*i.e.*, wide temperature range) of the annealing peak in that study suggests that the recovery peak was a superposition of several distinct annealing processes rather than a single process. Furthermore, Palomares et al. showed that most of the structural recovery in swift heavy ion irradiated ThO₂ was completed by $\sim 650 \text{ °C}$ [21]. The trend shown in Fig. 5 is consistent with both of these results. Most defects anneal between 275–575 °C, and the diffuse scattering reaches a minimum after 575 °C. The unit cell parameter recovers to the pre-irradiation value after annealing at 750 °C. Regarding the anomalous increase in diffuse scattering after 750 °C, this may be a result of sample heating. The sample was left to cool for at least 15 min prior to measurement. However, it is possible that the sample required a slightly longer cooling time after quenching from 750 °C. Analysis of the total scattering functions of the unirradiated sample showed that increasing the temperature causes the diffuse scattering to increase, and a broad band to appear between $\sim 1\text{--}2 \text{ \AA}$. The increase in diffuse scattering observed after the 750 °C annealing step is therefore attributed to an increase in intrinsic thermal disorder and is not related to defect annealing.

3.3. Raman spectroscopy

In order to better resolve the observed annealing stage(s), the sample was further characterized by Raman spectroscopy. Raman spectroscopy is a powerful method for probing the local structure of both ordered and disordered materials. Thus, insights gained from Raman spectroscopy are complimentary to the atomic structure information obtained from neutron total scattering. Fig. 6 shows the Raman spectra of ThO₂ before and after irradiation, and after annealing at 750 °C. The Raman spectrum of the unirradiated sample has a single peak at 465 cm^{-1} , in agreement with prior studies [19,29,30]. This feature corresponds to the triply-degenerate F_{2g} Raman-active optical phonon, which represents the symmetric breathing mode of the oxygen cage around each cation [30].

Swift heavy ion irradiation results in the formation of defects that distort the local structure causing the breakdown of the Raman-active selection rules [19]. A comparison of the unirradiated and as-irradiated (pre-annealing) spectra shows that the irradiation decreases the signal-to-noise ratio and modifies the F_{2g} peak properties. The F_{2g} peak of irradiated ThO₂ is red-shifted and broadens asymmetrically to the lower-frequency side. Similar asymmetric broadening of the F_{2g} peak has been observed in swift heavy ion-irradiated CeO₂ [31] and ThO₂-UO₂ solid solutions [29], and is indicative of a disruption of translational symmetry. The shift of the F_{2g} band to lower frequencies also suggests an elongation of the $\langle \text{Th-O} \rangle$ distance, which is consistent with volumetric swelling measured by XRD [11,19] and the results obtained from

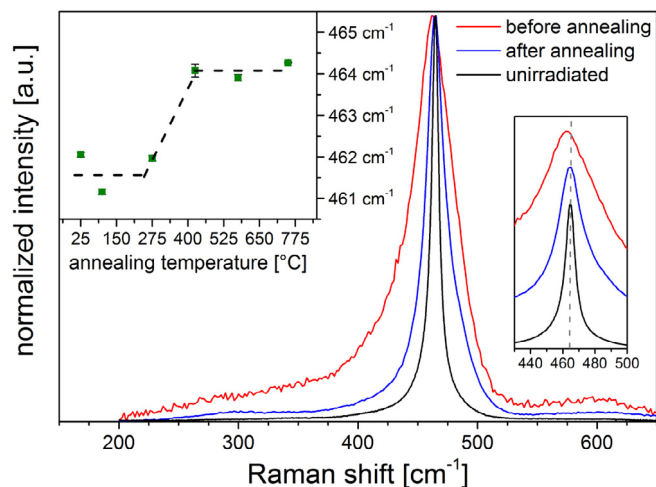


Fig. 6. Normalized Raman spectra of unirradiated ThO₂ (black), and irradiated ThO₂ (2-GeV Au ions, 1×10^{13} ions/cm²) collected prior to annealing (red) and after annealing at 750 °C for 20 min (blue). The Raman spectra collected for the other isochronal annealing temperatures are omitted for clarity. The insets show the position of the F_{2g} band as a function of isochronal annealing temperature. (For interpretation of the references to colour in this figure legend, the reader is referred to the web version of this article.)

pair distribution function analysis of swift heavy ion irradiated ThO₂ [12].

In addition to the modifications to the F_{2g} band, the spectrum of the irradiated sample also exhibits a broad band centered at ~ 600 cm⁻¹. This peak, or superposition of peaks, was previously observed in the spectra of ThO₂ irradiated at higher ion fluences with 945-MeV Au ions [19]. Similar features have also been identified in oxidized [32] and ion irradiated [33] UO₂. In the case of UO₂, this feature was attributed to the nondegenerate F_{1u} LO mode, which becomes Raman-active as a result of increased atomic disorder. However, Mohun et al. have shown that the intensity of the band at ~ 600 cm⁻¹ in energetic ion irradiated ThO₂ depends on the excitation wavelength (532 nm vs. 633 nm) [9]. Therefore, it is likely that the feature is caused by defect-induced photoluminescence. Varying the excitation wavelength from 532 nm to 473 nm did not yield any noticeable change in the satellite peak intensity and position. However, it is possible that the use of an excitation source with a longer wavelength is needed in order to reproduce the photoluminescence-related variation.

Isochronal annealing of the irradiated sample results in sharpening of the F_{2g} peak and an increase in the Raman signal-to-noise ratio. The width of the F_{2g} peak decreases continuously as a function of isochronal annealing temperature. This is in contrast to the position of the F_{2g} peak maximum, which shows a discontinuity between 275 and 425 °C (Fig. 6 inset). The discontinuity in peak position can be attributed to the first annealing event that was observed in the diffuse scattering data in the same temperature range. Further annealing after the 425 °C temperature step does not yield any noticeable change in the F_{2g} peak position. Unlike the unit cell parameter, the position of the F_{2g} peak does not recover to the pre-irradiation value (465 cm⁻¹) after annealing at the highest annealing temperature, 750 °C. This suggests that some local structural distortions persist in the material up to the highest temperature achieved in this study.

4. Discussion

The evolution of the unit cell parameter, the diffuse scattering, and the Raman spectroscopy data all indicate the presence of an annealing event between 275 and 425 °C. In order to ascertain its

origin, it is important to consider the defect structure that is present in ThO₂. Swift heavy ion irradiation of ThO₂ results in the formation of cylindrical damage zones along the trajectories of individual ions, called ion tracks. These features have been observed in ThO₂ directly with transmission electron microscopy (TEM) [34] and indirectly with XRD [11]. Ion tracks in ThO₂ exhibit a relatively disordered core region and a halo region, near the circumference of the track cross-sections, with fewer defects, but significant microstrain [19]. Tracy et al. [19] proposed that defect clusters in these tracks exhibit a radial size distribution, based on similar track structures that have been observed in fluorite-type alkali-halides [35]. In both ThO₂ and alkali-halides, it is expected that larger defect aggregates are concentrated at the core of the ion track whereas more isolated point defects and/or color centers populate the halo region.

The first annealing stage (275–425 °C) is characterized by several features: a noticeable change in the unit cell parameter, a discrete drop in diffuse scattering, and a shift in the F_{2g} peak in the Raman spectrum. Irradiated ThO₂ often exhibits large concentrations of color centers. Therefore, it was considered that the annealing stage is caused by the thermally-induced annihilation of these color centers at high temperature [8,36]. The color center concentration has been shown to have a significant effect on the unit cell parameter in alkali-halides, such as LiF [37,38]. However, the effect of color center annihilation in the present study is likely negligible because the ThO₂ sample showed minimal coloration after irradiation. It is possible that coloration was limited by the large concentration of grain boundaries in the loosely compacted samples ($\sim 60\%$ theoretical density).

The Raman spectrum of ThO₂ is highly influenced by the oxygen sublattice and less so by the cation sublattice. This is evidenced by the similarity in the Raman spectra of the various fluorite structures (e.g., CeO₂, ThO₂, PuO₂, and NpO₂) [39]. As such, the discrete shift of the F_{2g} peak observed here suggests that the first annealing event is associated with the annihilation of oxygen-type defects, such as oxygen Frenkel-type and/or oxygen cluster defects. The annealing stage (275–425 °C) is close in temperature to the oxygen migration regime in similar fluorite-structure oxides. Madier et al. have shown that oxygen becomes mobile in isostructural CeO₂ at ~ 400 °C [40]. Moreover, the fixed valence of thorium [41] combined with the low formation [42,43] and migration [44] energies of oxygen defects make anion disorder the preferred mode of defect incorporation in ThO₂. In addition to smaller point defects, such as anion Frenkel pairs, ThO₂ exhibits a tendency to accommodate charged defects [44] and oxygen defect agglomerates, such as dimers and peroxide ions [44–46]. Peroxide ions are bound states of two oxygen interstitials with an overall charge state of -2 [47]. These defects were experimentally identified in swift heavy ion irradiated CeO₂ [12], and are predicted to exist in non-stoichiometric ThO₂ [46].

Numerous studies on isostructural actinide oxides (UO₂, PuO₂) irradiated with neutrons [48–52] and alpha-particles [53,54] recorded similar isochronal annealing trends consisting of two prominent annealing stages. The first stage typically occurs between ~ 200 – 400 °C whereas the second stage occurs above ~ 500 °C. Weber compared the behavior of alpha-particle irradiated fluorite-structured materials and attributed these stages to the annealing of oxygen interstitials and cation vacancies, respectively [53]. This interpretation was corroborated by Matzke and collaborators for ion implanted UO₂ (see Ref. [55] and references therein). The first event observed between 275 and 425 °C is therefore attributed to the annealing of oxygen point defects and small oxygen defect aggregates, such as dimers and peroxide ions. The dissociation of larger interstitial-type defect clusters within the swift heavy ion track core between 275 and 425 °C is considered unlikely because these defects show evidence of high temperature sta-

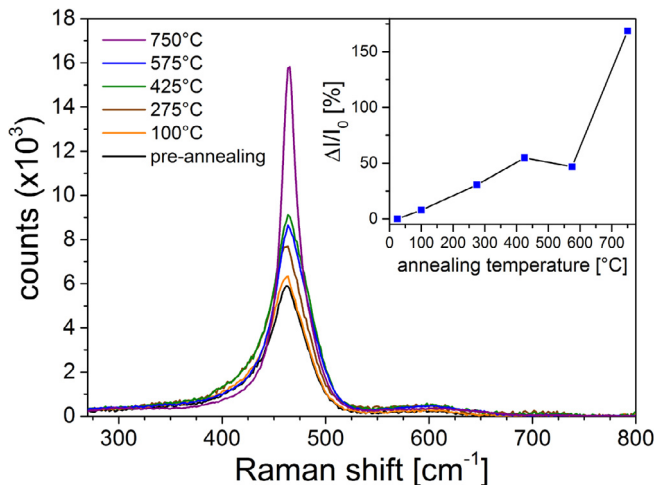


Fig. 7. Raman spectra of irradiated ThO₂ in absolute scale before and after annealing. The Raman spectra were collected from an identical spot on the sample. The inset shows the relative change in the F_{2g} peak maximum intensity as a function of isochronal annealing temperature.

bility. For example, Douglass et al. have shown that black-dot defects (ascribed to defect clusters and unresolvable loops) in alpha-irradiated ThO₂ are stable even after heating to 900 °C for 8 h [4]. At higher temperatures (~1300 °C), the black-dot defects act as nucleation sites for the coalescence and growth of larger defect clusters and dislocation loops [4,56].

Interestingly, the shift of the F_{2g} peak does not show evidence for the second annealing event at higher temperatures, as the wavenumber position of the F_{2g} peak does not shift significantly following annealing at temperatures above 425 °C. The only change in the Raman spectra is a ~80% increase in the F_{2g} peak intensity between the 575 °C and 750 °C temperature steps (Fig. 7). For comparison, the change in F_{2g} peak intensity from 25–575 °C was only about 50%. The notable change in F_{2g} peak intensity between 575 and 750 °C may be attributed to the second annealing stage of cation vacancy migration and recovery, as suggested by Weber [53] and Matzke [55]. Following these studies, the large change in the F_{2g} peak intensity between 575 and 750 °C is tentatively attributed to the annihilation of cation vacancy defects considering that the maximum F_{2g} peak intensity likely increases as cation defects are annealed and ThO₈ polyhedra recover to near-pristine arrangement. The change in the Raman signal-to-noise ratio in this temperature regime is in agreement with the diffuse scattering and unit cell parameter data, which show continued annealing up to 750 °C. However, further experiments are needed to unequivocally confirm the cation vacancy annealing stage. Analysis of the ion track structure in ThO₂ using high-angle annular dark-field scanning transmission electron microscopy (HAADF-STEM) [6] can provide further insight for determining the extent of disordering on the cation sublattice in order to further elucidate the defect structure of swift heavy ion irradiated ThO₂.

5. Conclusions

The structural recovery of ThO₂ irradiated with 2-GeV Au ions was investigated by means of isochronal annealing, neutron total scattering, and Raman spectroscopy. Rietveld refinement of the neutron diffraction patterns shows that the unit cell parameter monotonically decreases as a function of isochronal annealing temperature, recovering to the pre-irradiation value by 750 °C. The neutron total scattering functions also indicate that the Bragg scattering from crystalline domains in the irradiated ThO₂ sample

increases, relative to the diffuse scattering, as the sample is annealed to higher temperatures. The diffuse neutron scattering and Raman spectroscopy measurements indicate that a substantial isochronal annealing stage occurs between ~275–425 °C. The annealing event is attributed to the annihilation of oxygen point defects and small oxygen defect clusters.

Acknowledgements

This research is funded by the Office of Basic Energy Sciences of the U.S. Department of Energy as part of the *Materials Science of Actinides* Energy Frontier Research Center (DE-SC0001089). The research at ORNL's Spallation Neutron Source was sponsored by the Scientific User Facilities Division, Office of Basic Energy Sciences, U.S. Department of Energy. R.I.P. gratefully acknowledges support from the U.S. Department of Energy (DOE) National Nuclear Security Administration (NNSA) through the Carnegie DOE Alliance Center (CDAC) under Grant number DE-NA-0002006. The authors thank Jacob Shamblin, Brandon Perlov, and Jason Behrens for assistance with the neutron scattering measurements.

References

- [1] IAEA, Thorium Fuel Cycle – Potential Benefits and Challenges TECDOC-1450. 2005: Vienna, Austria.
- [2] M. Lung, O. Gremm, *Perspectives of the thorium fuel cycle*, Nucl. Eng. Des. 180 (2) (1998) 133–146.
- [3] D.M. Duffy, S.L. Daraszewicz, J. Mulroue, Modelling the effects of electronic excitations in ionic-covalent materials, Nucl. Instrum. Methods Phys. Res. Sect. B 277 (2012) 21–27.
- [4] D.L. Douglass, S.E. Bronisz, Alpha particle irradiation damage in ThO₂, J. Am. Ceram. Soc. 54 (3) (1971) 158–161.
- [5] C.A. Yablinsky et al., Characterization of swift heavy ion irradiation damage in ceria, J. Mater. Res. 30 (9) (2015) 1473–1484.
- [6] S. Takaki et al., Atomic structure of ion tracks in Ceria, Nucl. Instrum. Methods Phys. Res. Sect. B 326 (2014) 140–144.
- [7] K. Yasuda et al., Defect formation and accumulation in CeO₂ irradiated with swift heavy ions, Nucl. Instrum. Methods Phys. Res. Sect. B 314 (2013) 185–190.
- [8] B.G. Childs, P.J. Harvey, J.B. Hallett, Color centers and point defects in irradiated thoria, J. Am. Ceram. Soc. 53 (8) (1970) 431–435.
- [9] R. Mohun et al., Charged defects during alpha-irradiation of actinide oxides as revealed by Raman and luminescence spectroscopy, Nucl. Instrum. Methods Phys. Res., Sect. B 374 (2016) 67–70.
- [10] V.I. Neeley, J.B. Gruber, W.J. Gray, F_{2g} centers in thorium oxide, Phys. Rev. 158 (3) (1967) 809–813.
- [11] C.L. Tracy et al., Redox response of actinide materials to highly ionizing radiation, Nat. Commun. 6 (2015) 6133.
- [12] R.I. Palomares et al., Defect accumulation in swift heavy ion-irradiated CeO₂ and ThO₂. submitted for publication.
- [13] J.F. Ziegler, M.D. Ziegler, J.P. Biersack, SRIM – The stopping and range of ions in matter (2010), Nucl. Instrum. Methods Phys. Res. Sect. B 268 (11–12) (2010) 1818–1823.
- [14] M.I. Lang et al., Swift heavy ion-induced phase transformation in Gd₂O₃, Nucl. Instrum. Methods Phys. Res. Sect. B 326 (2014) 121–125.
- [15] J. Neufeind et al., The Nanoscale Ordered Materials Diffractometer NOMAD at the Spallation Neutron Source SNS, Nucl. Instrum. Methods Phys. Res., Sect. B 287 (2012) 68–75.
- [16] B.H. Toby, R.B. Von Dreele, GSAS-II: the genesis of a modern open-source all purpose crystallography software package, J. Appl. Crystallogr. 46 (2) (2013) 544–549.
- [17] C.L. Farrow et al., PDFfit2 and PDFgui: computer programs for studying nanostructure in crystals, J. Phys. Condens. Matter 19 (33) (2007).
- [18] K. Syassen, DATLAB, version 1.29. MPI/FKF: Stuttgart, Germany.
- [19] C.L. Tracy et al., Defect accumulation in ThO₂ irradiated with swift heavy ions, Nucl. Instrum. Methods Phys. Res. Sect. B 326 (2014) 169–173.
- [20] C.L. Tracy et al., Review of recent experimental results on the behavior of actinide-bearing oxides and related materials in extreme environments, Prog. Nucl. Energy (2016).
- [21] R.I. Palomares et al., In situ defect annealing of swift heavy ion irradiated CeO₂ and ThO₂ using synchrotron X-ray diffraction and a hydrothermal diamond anvil cell, J. Appl. Crystallogr. 48 (2015) 711–717.
- [22] X. Qiu et al., Reciprocal-space instrumental effects on the real-space neutron atomic pair distribution function, J. Appl. Crystallogr. 37 (1) (2004) 110–116.
- [23] J.W. Corbett, R.M. Walker, Discrete recovery spectrum below 65°K in irradiated copper, Phys. Rev. 110 (3) (1958) 767–768.
- [24] W. Primak, Kinetics of processes distributed in activation energy, Phys. Rev. 100 (6) (1955) 1677–1689.

- [25] V.M. Niels, D.A. Keen, *Diffuse Neutron Scattering from Crystalline Materials*, first ed., Oxford Series on Neutron Scattering in Condensed Matter, Oxford University Press, 2001, 336.
- [26] S. Hull et al., Oxygen vacancy ordering within anion-deficient Ceria, *J. Solid State Chem.* 182 (10) (2009) 2815–2821.
- [27] G. King et al., Local structure of the vacancy disordered fluorite Yb_3TaO_7 from neutron total scattering, *J. Mater. Chem. A* 1 (35) (2013) 10487–10494.
- [28] J. Shamblin et al., Probing disorder in isometric pyrochlore and related complex oxides, *Nat. Mater.* 15 (5) (2016) 507–511.
- [29] R. Rao et al., Raman spectroscopic investigation of thorium dioxide-uranium dioxide ($\text{ThO}_2\text{-UO}_2$) fuel materials, *Appl. Spectrosc.* 68 (1) (2014) 44–48.
- [30] V.G. Keramidis, W.B. White, Raman spectra of oxides with the fluorite structure, *J. Chem. Phys.* 59 (3) (1973) 1561–1562.
- [31] K. Ohhara et al., Oxygen defects created in CeO_2 irradiated with 200 MeV Au ions, *Nucl. Instrum. Methods Phys. Res., Sect. B* 267 (6) (2009) 973–975.
- [32] H. He, D. Shoesmith, Raman spectroscopic studies of defect structures and phase transition in hyper-stoichiometric UO_2+x , *Phys. Chem. Chem. Phys.* 12 (28) (2010) 8108–8117.
- [33] G. Guimbretiere et al., Determination of in-depth damaged profile by Raman line scan in a pre-cut He^{2+} irradiated UO_2 , *Appl. Phys. Lett.* 100 (25) (2012).
- [34] J.H. Chute, Direct observation of fission fragment damage in some ceramic oxides, *J. Nucl. Mater.* 21 (1) (1967) 77–87.
- [35] N.A. Medvedev et al., Effect of spatial redistribution of valence holes on the formation of a defect halo of swift heavy-ion tracks in LiF, *Phys. Rev. B* 87 (10) (2013).
- [36] T.R. Griffiths, J. Dixon, Electron irradiation of single crystal thorium dioxide and electron transfer reactions, *Inorg. Chim. Acta* 300–302 (2000) 305–313.
- [37] J.Z. Damm, J. Stepień-Damm, Effect of γ -irradiation on the lattice parameter and colour centre concentration in pure Ca^{2+} , Sr^{2+} and Eu^{2+} doped KCl crystals, *Kristall und Technik* 15 (10) (1980) 1167–1172.
- [38] R. Balzer, H. Peisl, W. Waidelich, Gitterfehlordnung in KCl mit Farbzentren, *Zeitschrift für Physik A Hadrons and nuclei* 204 (4) (1967) 405–418.
- [39] M.J. Sarsfield et al., Raman spectroscopy of plutonium dioxide and related materials, *J. Nucl. Mater.* 427 (1–3) (2012) 333–342.
- [40] Y. Madier et al., Oxygen mobility in CeO_2 and $\text{CexZr}(1-x)\text{O}_2$ compounds: study by CO transient oxidation and $^{18}\text{O}/^{16}\text{O}$ isotopic exchange, *J. Phys. Chem. B* 103 (50) (1999) 10999–11006.
- [41] G.E. Murch, C.R.A. Catlow, Oxygen diffusion in UO_2 , ThO_2 and PuO_2 – a review, *J. Chem. Soc.-Faraday Trans. II* 83 (1987) 1157–1169.
- [42] E.A. Colbourn, W.C. Mackrodt, The calculated defect structure of thoria, *J. Nucl. Mater.* 118 (1) (1983) 50–59.
- [43] Y.S. Yun, W.W. Kim, First principle studies on electronic and defect structures of UO_2 , ThO_2 , and PuO_2 , in: *Proceedings of the KNS spring meeting, 2007*, Korea, Republic of: KNS.
- [44] H.Y. Xiao, Y. Zhang, W.J. Weber, Stability and migration of charged oxygen interstitials in ThO_2 and CeO_2 , *Acta Mater.* 61 (20) (2013) 7639–7645.
- [45] S.T. Murphy, M.W.D. Cooper, R.W. Grimes, Point defects and non-stoichiometry in thoria, *Solid State Ionics* 267 (2014) 80–87.
- [46] S.C. Middleburgh, G.R. Lumpkin, R.W. Grimes, Accommodation of excess oxygen in fluorite dioxides, *Solid State Ionics* 253 (2013) 119–122.
- [47] S.C. Abrahams, J. Kalnajs, The crystal structure of barium peroxide, *Acta Crystallogr. A* 7 (12) (1954) 838–842.
- [48] J. Bloch, Restauration thermique du parametre de l' uo_2 faiblement irradie, *J. Nucl. Mater.* 3 (2) (1961) 237–238.
- [49] J.R. Macewan, R.L. Stoute, Annealing of irradiation-induced thermal conductivity changes in ThO_2 -1.3 wt percent UO_2 , *J. Am. Ceram. Soc.* 52 (3) (1969) 160.
- [50] N. Nakae, Y. Iwata, T. Kirihaara, Thermal recovery of defects in neutron-irradiated UO_2 , *J. Nucl. Mater.* 80 (2) (1979) 314–322.
- [51] N. Nakae, Y. Iwata, T. Kirihaara, Thermal recovery of defects in neutron irradiated UO_2 , *J. Nucl. Mater.* 80 (2) (1979) 314–322.
- [52] N. Nakae et al., Irradiation induced lattice defects in UO_2 , *J. Nucl. Mater.* 71 (2) (1978) 314–319.
- [53] W.J. Weber, Alpha-irradiation damage in CeO_2 , UO_2 and PuO_2 , *Radiat. Eff. Defects Solids* 83 (1–2) (1984) 145–156.
- [54] S.D. Günay, Thermal Recovery Mechanisms of UO_2 Lattices. ArXiv e-prints, 2016. 1605: p. arXiv:1605.05831.
- [55] H. Matzke, Atomic transport-properties in UO_2 and mixed oxides (U, Pu) O_2 , *J. Chem. Soc. -Faraday Trans. II* 83 (1987) 1121.
- [56] F.W. Clinard, D.L. Douglass, C.C. Land, Strain effects and spalling in alpha-bombarded ThO_2 , *J. Am. Ceram. Soc.* 54 (4) (1971) 177–179.